Hindawi
Advances in Civil Engineering
Volume 2023, Article ID 6629970, 18 pages
https://doi.org/10.1155/2023/6629970

Review Article

Dynamic Behaviors of Fiber-Reinforced Cellular Concrete Fabricated with Millimeter-Sized Superabsorbent Polymer

Junru Ren, Ling Zhou, Chaoshan Yang, Rui Mu, Lei Mao, and Yuhao Zhu

Army Logistic Academy, North First Road 20 of University Town, Chongqing, China

Correspondence should be addressed to Ling Zhou; zhouling830@163.com

Received 27 June 2023; Revised 17 September 2023; Accepted 28 September 2023; Published 8 November 2023

Academic Editor: S. H. Chu

A novel cellular concrete with millimeter-level pores fabricated with superabsorbent polymers and fiber is introduced. Porous structure with reinforcement of fiber are adopted to improve crack resistance and shock-absorbing ability. To investigate the dynamic mechanical performance of fiber-reinforced cellular concrete, quasistatic compression and split Hopkinson pressure bar tests with strain rate from 15 to 90 s^{-1} were conducted. Three different fiber volume fractions (0.2%, 0.6%, and 1%), and two types of fibers (polypropylene fiber and basalt fiber (BF)) were adopted. Along with two levels of porosities (20% and 60%), total of 12 mix designs of cellular concrete to three-level axial impacting. The research results show that the novel cellular concrete is sensitive to high strain rates, demonstrating increasing dynamic compressive strength, dynamic elastic modulus, dynamic increase factor (DIF), and peak toughness with the increase in strain rate. In addition to the inertia effect, the locally enhanced porous structure and fiber structure can change the stress field and crack path, along with the energy consumption of deformation and cracks in the pores. The amount of fiber, physicochemical property, distribution, and shape amplify or dampen through its thickening effect, interface reaction, and stress transmission. Recommended fiber types and dosages were proposed to improve strength, stiffness, and toughness. BF showed an enhanced performance in terms of strength, modulus, and sharp strain-rate effect. Rules of DIFs were also studied. Awareness of the dynamic properties provides a foundation for proper design of structural members and increases the use of cellular concrete.

1. Introduction

As the most widely used building material, concrete and its reinforcements must cope with accidental hazards, such as terrorist and bombing attacks. Under impact or blast loading, structural components exhibit vibration, penetration, and spalling, causing severe threat to human security. Furthermore, concrete experiences substantial deformation at high-level strain rates where stress waves are generated and propagated to crack until failure. Hence, modifying the dynamic performance of concrete is a fundamental and effective method to improve the safety of engineering structures.

Porous medium, generally, has the ability to attenuate and dissipate dynamic loads. Complicated transmission and reflection of stress waves occur at the interface of the matrix and inner air [1]. The collapse and crush of pores can consume dynamic energy [2]. Porous concrete is also applied as back fillings [3], featured with artificial macropores formed by expanded polystyrene (EPS) microspheres, hollow spheres, or foaming agents, which are completely distinct from the lacunas and holes of normal concrete. EPS microspheres deform and crumble to absorb dynamic energy with a content of 20–30 vol% [4]. Hollow corundum balls offered more toughness in the split Hopkinson pressure bar (SHPB) test, showing an evident platform stage in stress–strain curves [5]. Foam concrete of 800–900 kg/m^3 collapsed with layered compaction with strain rates over 500 s^{-1}. While increase in strength and deformation was not detected, the platform stage in stress–strain curves with strain rates under 60 s^{-1} [6–8]. Besides, 220 kg/m^3 foamed concrete exhibited a trapezoid dynamic stress–strain curve [9]. The aforementioned concrete presented an evident strain-rate effect with great dynamic increase factors (DIFs). Meanwhile, different loading intensity and mixture density produced various deformational and energy-absorbing behaviors.

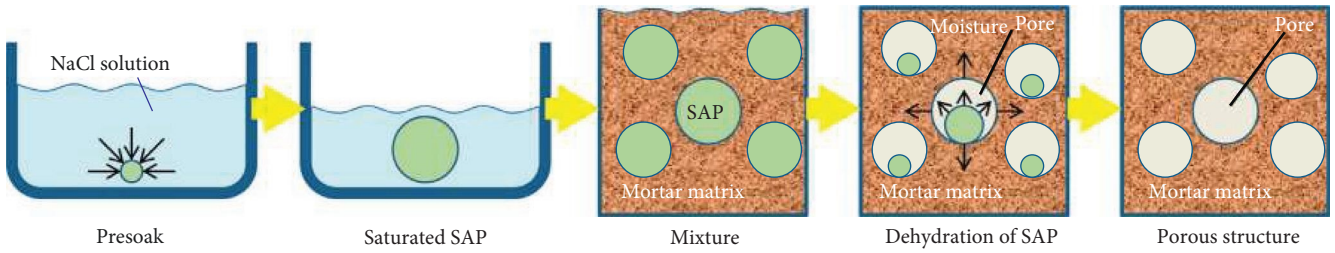

Figure 1: Fabrication of the cellular concrete with SAPs.

Fibers, including metal fiber and nonmetal fiber, can effectively relieve cracking and improve the toughness of concrete [10]. Metal fiber, such as steel fiber is usually employed in bulletproofs, which can significantly improve the tensile strength, toughness, and crack resistance of concrete matrix [11–13]. With the popularization of steel fiber reinforced concrete, current studies mainly focus on the packing of steel fiber-aggregate mixtures and the effect of steel fibers and prediction model [14, 15]. Nonmetal fiber, such as polypropylene fiber (PPF) and basalt fiber (BF), is applied in military fortifications to reduce local damage such as spalling for its high viscous effect as well as strength of tensile and shear [16–18]. Utilization of fibers prevented premature fracture and led to improved postcracking stiffness and ductility [19]. Reports found that high-modulus fiber enhances toughness by improving material strength and ductility. While low-modulus fiber could only increase the ductility of concrete. As for steel fiber reinforced concrete, the impact toughness and dynamic compressive stress increased with the increase of fiber content at the range of 0–6 vol%. Higher content (>3 vol%) significantly improves the strain-rate sensitivity, reaching 1.6–2.2 of dynamic strength growth, although the peak strain has no change [20, 21]. PPF can also mitigate the impact damage of concrete. With a low content of 0.05–0.3 vol%, fibers demonstrated superior thickening effect and cracking resistance. High fiber content could better toughen concrete and bridge cracks [22]. Experiments verified that more fiber (1–2 vol%) would damage the static strength of concrete due to its weak interfaces. Under a strain rate of 20–100 s^{-1}, optimum fiber content to improve dynamic strength and toughness should match the strength of concrete [21], thus more fiber should be added to high-strength concrete. Steel fiber, with higher modulus and strength, can improve strength and peak deformation to enhance the dynamic toughness of concrete. While, PPF mainly increases the ultimate deformation because of lower modulus and strength. Both fibers achieved greater ability of deformation and load holding before failure with increasing fiber content, acquiring a lower softening rate after peak deformation.

BF is a typical silicate fiber with desirable temperature tolerance, acid and alkali resistance, low water absorption, and lower cost than carbon fiber or glass fiber [16, 23]. Highlighted by higher tensile strength and modulus than PPF, experiments confirmed that cement mortar and concrete reinforced by BF both demonstrated a sharp strain-rate effect under dynamic loads with strain rates of 20–100 s^{-1} [24, 25]. With content of 0.1–0.3 vol%, all specimens reached higher dynamic toughness, which increased with strain rate, but did not show linear growth with fiber content. Specimens with fiber of 0.2 vol% under strain rate of 50–60 s^{-1} obtained the maximum improvement of toughness [24]. Compared to carbon fiber reinforced concrete, concrete with 0.1 vol% BF acquired greater increase of strength and toughness under strain rate of 20–100 s^{-1}. While more fiber made neither material obtained evident enhancement [25]. Therefore, the properties of the fibers are an inherent reason for the different dynamic behavior of concrete. The type of concrete, strength, stiffness, and dosage of fiber along with the strain rate caused coupling effects, resulting in various failure phenomenon and mechanical performance.

The evolution of stress waves in concrete is a coupling problem including wave feature and material characteristics [9]. Pore proportion and pore evolution play a major role for cellular concrete [26]. Besides the dynamic development of the solid matrix, pore structure led to the transmission and reflection of stress wave accompanied by energy dissipation. The solid medium bears the most dynamic stress, and the other acts on the pore interface and the surrounding medium. With the higher proportion of pores, more pore interfaces create more impedance variations, along with intensive reflection and subsequent overlapped waves, and increase the amplitude and the number of peaks of reflected waves. The irreversible deformation of pores and its surrounding matrix, including shape change, plastic deformation, and fracture, are also outlets of dynamic energy.

Figure 1 shows the proposed a novel method to fabricate cellular concrete through SAPs as inner molds [27]. Those spheres would construct a porous structure with closed discrete pores with diameter of 5–7 mm, which is believed to attenuate stress wave. Especially, the hydraulic reaction of cement was confirmed to continue in the surrounding surface leading to enhanced layer [28]. Different from EPS concrete and foamed concrete, cellular concrete is bound to possess distinctive dynamic behavior special inner structure. Allied with the strengthen effect of fibers, the fiber-reinforced novel cellular concrete might demonstrate great prospects in impact resistance.

In this study, the dynamic mechanical behavior of a novel cellular concrete with various fiber incorporated, SHPB tests at different strain rates were performed and three fiber volume fractions were adopted. The objective of this paper is to investigate the influence law and mechanism of pores and fibers on the dynamic compressive properties

Table 1: General properties of fibers.

Fiber	Polypropylene fiber	Basalt fiber
Density (g/cm^3)	0.91	2.65
Length (mm)	9	12
Tensile strength (MPa)	382.9	4,150
Ultimate deformation (%)	40	3.1
Diameter (μm)	51	15
Young's modulus (GPa)	4.9	93

including dynamic compressive strength, dynamic elastic modulus, DIF, and impact toughness. It may promote further understanding and application of cellular concrete in fields of building construction or shock absorption.

2. Experimental Work

2.1. Materials. Ordinary portland cement with an ultimate strength of 52.5 MPa and sulfate aluminum cement (SAC) with an ultimate strength of 42.5 MPa were used with a proportion of 9 : 1. SAC can promote the setting and hardening to avoid water loss of superabsorbent polymers (SAPs) and consequent bleeding. Concerning about the influence of particle-size distribution and bulk density on matrix strength, some ultrafine powder with pozzolanic effect such as silica fume (SF) and fly ash (FA) were added to fill up voids in the matrix and optimize the fluidity [29, 30]. SF with an average fineness of 0.15 μm, specific surface area of 21,575 m^2/kg, burning loss of 1.81%, SiO_2 content of 95.5%, and 28 days active index of 118% was utilized. FA with average fineness of 6.5 μm, combustion loss of 2.8, and CaO content of 4% was employed. Fine aggregates were river sand with a fineness modulus of 1.65. Liquid polycarboxylic acid superplasticizer was dissolved in water to reduce undesired voids. The mix water is normal tap water, while the SAPs were presoaked in NaCl solution with a concentration of 1 mol/L to reach an average sphere diameter of 5–7 mm. The general properties of PPF and BF are presented in Table 1.

2.2. Mixture Designs. As shown in Tables 2 and 3, twelve mixtures of cellular concrete were designed with two levels of porosity, two fiber types, and three fiber dosages chosen as variables of the cellular concrete. Cellular concrete with 20% porosity can be applied in building structures. Higher-porosity cellular concrete can be applied as backfill and cushioning. PPF and BF were selected with significant difference in modulus and strength (Table 1). The fiber dosages were set as 0.2, 0.6, and 1 vol%. relative to the volume of the mortar matrix. All series of specimens shared the concrete matrix in Table 2, while different fiber was added.

The principal factors affecting the strength of the cellular concrete are sand–cement ratio, SF content, and water–cement ratio. Based on repeated tests, the relative parameters of the cellular concrete with porosity of 20% were sand–cement ratio of 0.89, SF content of 25 wt%, and water–cement ratio of 0.22. As for cellular concrete with porosity of 60%, the water–cement ratio was reduced to 0.18 for the self-absorbed water on SAPs.

Table 2: Mixture proportions for cellular concrete with various porosities (kg/m^3).

Porosity	OPC	SAC	Sand	SF	FA	W	PC	Sat-SAP
20%	769.6	85.5	761	213.8	17.1	188.1	17.1	137.8
60%	481	53.4	475.6	133.6	10.7	122.2	5.3	344.5

2.3. Specimens. Nine cylinder specimens of each design, total of 108 specimens, were fabricated with a size of $\Phi 70 \times 35$ mm. Specimens of each mix design were exposed to three levels of strain rate controlled by impacting velocity of SHPB. Every three specimens were subjected to replicated tests to avoid operating errors. Meanwhile, 36 cylinder specimens with a size of $\Phi 140 \times 35$ mm were made exposed to quasi-static loading. After pouring and 28-day standard curing, the two ends of the specimen were polished with a deviation of surface flatness less than 0.02 mm (Figure 2).

2.4. Experimental Setup

2.4.1. Quasistatic Uniaxial Compressive Test. A universal tester with a range of 300 kN was used to apply stable deformation with a strain rate lower than 3.5×10^{-5} s^{-1} on the cellular concrete specimen. The loading regime consisted of preloading and standard with the same loading of 4.9×10^{-3} mm/s. A preload of 5 kN was employed first and then unload to check the support and tight contact of all components. The standard load was continuous loading till failure.

2.4.2. SHPB Test. SHPB is a device to indirectly acquire dynamic strain–stress curves of solid material under impact by measuring the elastic wave history of pressure bars rather than directly measuring specimens undergoing rapid deformation and cracking. As shown in Figure 3, the SHPB device with a main diameter of 74 mm in this experiment consists of pneumatic system, impact rod, incident and transmitted bars, absorption bar and damping system, data acquisition and processing system. The impact rod and pressure bars are made of alloy steel with elastic modulus of 210 GPa and yield stress of 400 MPa. The sample is placed between two pressure bars to attain an uniaxial dynamic compression. Vaseline was put on the contact surfaces to reduce the effects of interfacial friction [31]. A rubber pulse sharper with a size of $\Phi 10 \times 1.1$ mm was utilized to relieve the dispersion of the incident wave and extend the time of the rising edge.

Three levels of strain rate were achieved by three conditions of impacting velocity, meaning three levels of inflation pressures of 0.15, 0.34, and 0.58 MPa, corresponding to velocities of 8.0, 14.4, and 20.5 m/s, respectively. The typical stress waves of the same specimen under three conditions of impact loading are presented in Figure 4.

2.5. Measuring Methods and Data Process. As shown in Figure 3, incident and reflected strain histories (ε_i and ε_r) were recorded by strain gauges on the incident bar. Transmitted strain histories (ε_t) were recorded by strain gauges on

Table 3: All series of specimens with various fiber type and dosage.

ID	Porosity	Fiber type	Fiber (vol%)	Fiber mass (kg/m^3)	ID	Porosity	Fiber type	Fiber (vol%)	Fiber mass (kg/m^3)
K1	20%	PPF	0.2	1.46	K7	60%	PPF	0.2	0.91
K2	20%	PPF	0.6	4.38	K8	60%	PPF	0.6	2.74
K3	20%	PPF	1	7.3	K9	60%	PPF	1	4.56
K4	20%	BF	0.2	4.24	K10	60%	BF	0.2	2.65
K5	20%	BF	0.6	12.72	K11	60%	BF	0.6	7.95
K6	20%	BF	1	21.2	K12	60%	BF	1	13.25

(a) (b)

Figure 2: Cross section of novel cellular concrete. (a) porosity = 20% and (b) porosity = 60%.

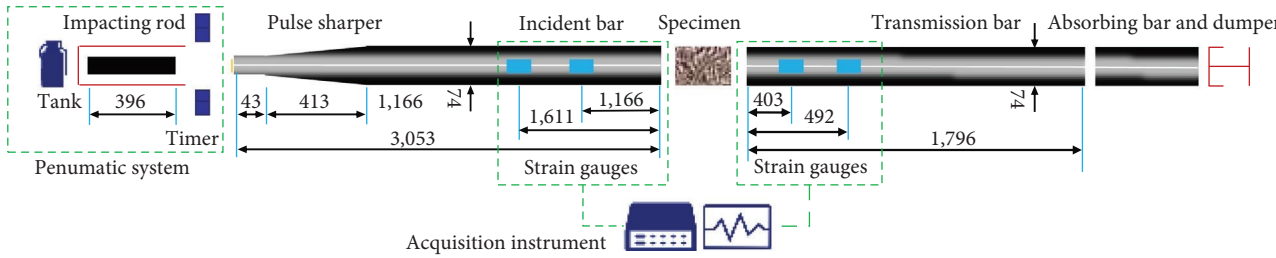

Figure 3: Bar size and strain gauge position.

the transmission bar. To reduce errors from bending of pressure bars, two strain gauges were connected in a half-bridge method and spaced by 180° on one pressure bar.

2.5.1. Stress–Strain History. As shown in Equation (1), the recorded data was analyzed by the "two wave" method to acquire strain–stress curves of specimens. The stress–strain curves obtained from each test are smooth without oscillation and have good coincidence. The curves in Figures 5–12 are the average of the three test curves.

$$\begin{cases} \dot{\varepsilon} = -\dfrac{2C_0}{L_s}\varepsilon_r(t) \\ \varepsilon = -\dfrac{2C_0}{L_s}\displaystyle\int_0^t \varepsilon_r(t)dt\,, \\ \sigma = \dfrac{A_0}{A_s}E_0\varepsilon_t(t) \end{cases} \tag{1}$$

where C_0, A_0, and E_0 are the velocity of elastic stress wave, section area, and elastic modulus, respectively, and A_s was the section area of the specimen.

2.5.2. Strain Rate. The instant strain rate of the specimen is the derivative of $\varepsilon(t)$, which changes rapidly. The average strain rate $\dot{\varepsilon}_1$ of the upward stage of stain history was analyzed, which was defined as $\dot{\varepsilon}_1 = \varepsilon_p/\Delta t$. ε_p was peak strain corresponding to the peak stress σ_p. Δt was the time from the start point to the peak strain.

2.5.3. Dynamic Elastic Modulus. As shown in Equation (2), the dynamic elastic modulus was defined as the average modulus between the point of 10% peak stress to 30% peak stress of the upward stage.

$$E = \frac{\sigma_b - \sigma_a}{\varepsilon_b - \varepsilon_a}, \tag{2}$$

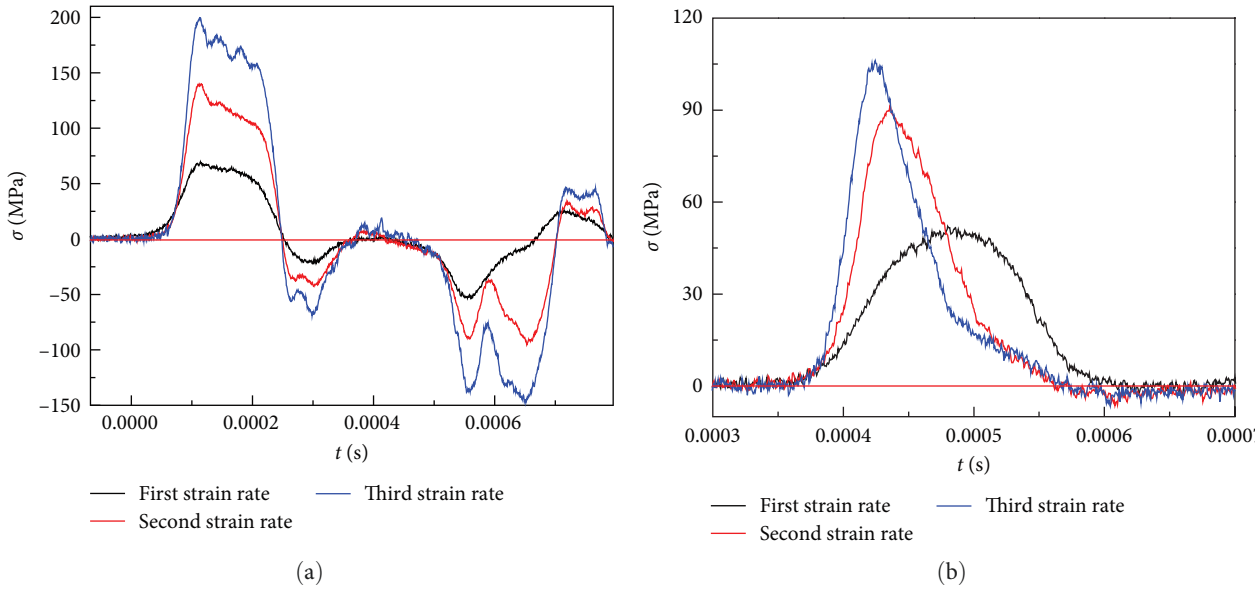

Figure 4: Typical stress histories recorded in the test. (a) Typical incident and reflected wave and (b) typical transmitted waves.

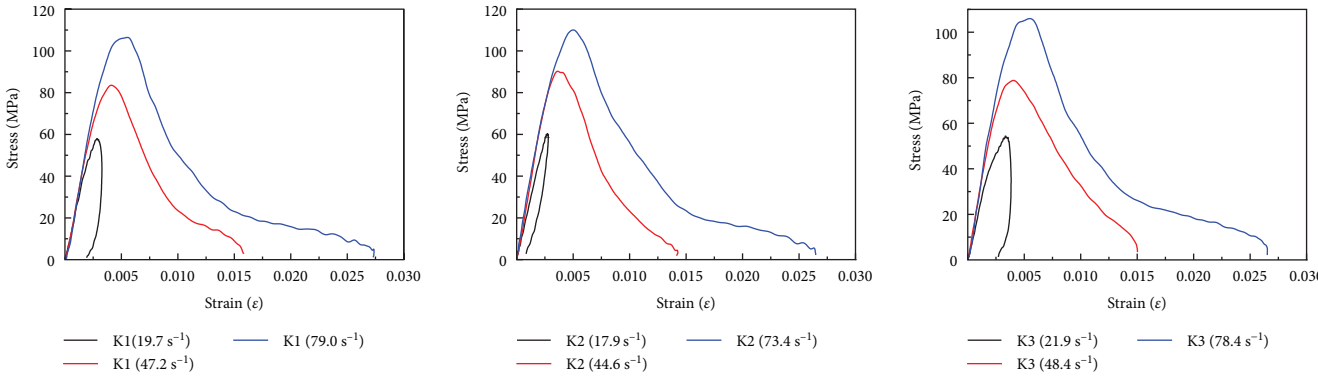

Figure 5: Dynamic stress–strain curves of cellular concrete with 20% porosity and PPF.

where σ_a and σ_b were, respectively, $10\%\sigma_p$ and $30\%\sigma_p$ of upward stage, ε_a and ε_b were the corresponding strain.

2.5.4. Impact Toughness. As shown in Equation (3) and Figure 13, peak toughness refers to the area enclosed by the stress–strain curve and coordinate axes from the origin to the peak stress point to analyze the energy absorption from loading to failure.

$$R = \int_0^{\varepsilon_p} \sigma d\varepsilon. \tag{3}$$

2.5.5. DIFs. DIF was originally proposed by the Euro-International Committee for Concrete (CEB) to describe dynamic increasing behaviors of concrete plainly using the ratio of dynamic indicators to quasi indicators. The DIFs of compressive strength, modulus, and toughness were defined as follows:

$$\text{DIF} - f_C = \frac{f_{\text{dynamic},c}}{f_{\text{quasi},c}}, \ \text{DIF} - E = \frac{E_{\text{dynamic},c}}{E_{\text{quasi},c}}, \text{DIF} - R = \frac{R_{\text{dynamic},c}}{R_{\text{quasi},c}}. \tag{4}$$

3. Results and Discussion

3.1. Failure Mode. As shown in Figure 14, four scenarios of failure phenomena were observed: slight-spalling, breaking, fragmentation, and comminution.

With an increase in load, the specimen demonstrated a gradually intensified trend from minor cracks to crush. Under dynamic compression, the development of the main cracks lagged behind the germination of minor cracks. Therefore, the fragments were more numerous and smaller under higher strain-rate deformation. A higher fiber content could possibly maintain the integrity of the specimen.

This "anticracking" effect is more evident in the cellular concrete with low porosity. For the 20% porosity cellular concrete, PPF provided better cracking resistance than BF.

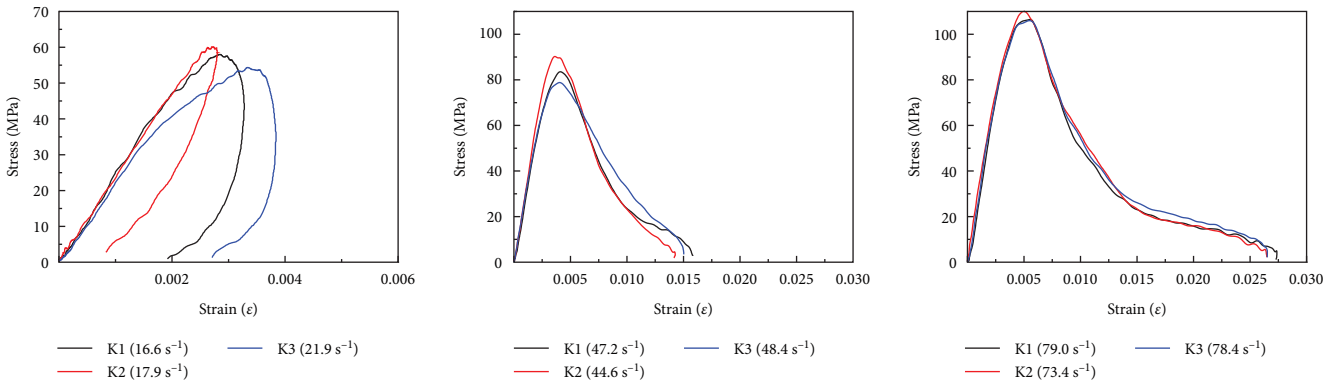

Figure 6: Effect of PPF content in cellular concrete with 20% porosity under the same loading.

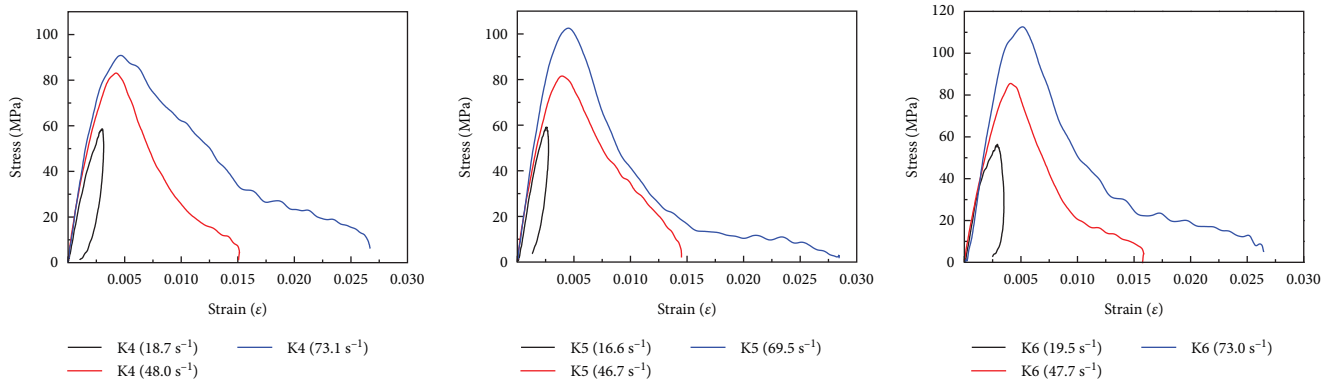

Figure 7: Dynamic stress–strain curves for cellular concrete with 20% porosity and BF.

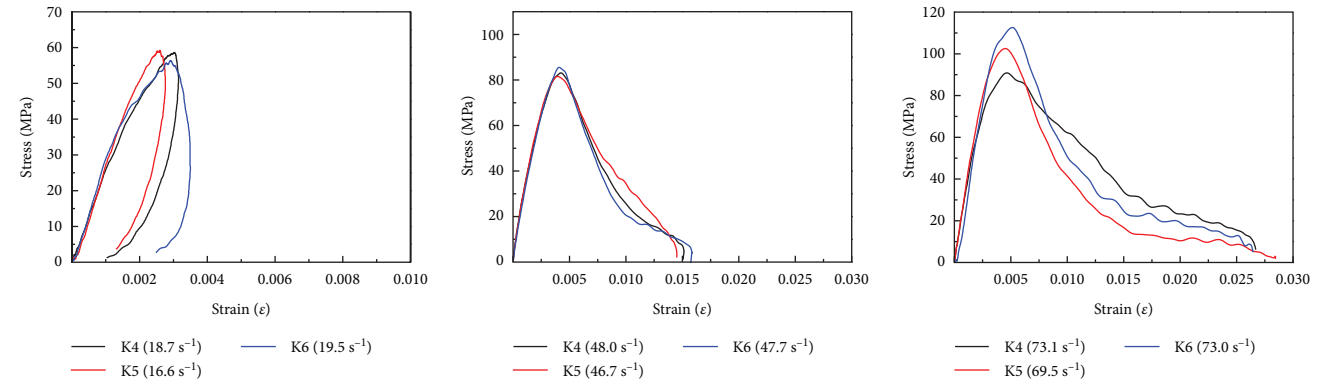

Figure 8: Effect of BF content in cellular concrete with 20% porosity under the same loading.

Under the same load, specimens with 60% porosity demonstrated more severe damage and cracks. The addition of fiber had little effect on mitigating damage, especially under a high strain-rate deformation.

As shown in Figure 15, the fibers exhibited different shapes in the 3D pore structure of the cellular concrete. Because fiber is longer than the sphere diameter of SAPs, it may bend in (①) or pass through (②) the cement mortar. However, this is not conducive to the cracking resistance and produces initial defects in the ideal shape of fiber (③), through the weakening of the anchorage between fiber and matrix. The amount of cement mortar matrix decreases with the increase of porosity, which means less solid medium to directly transfer and bear loading and a shorter distance for cracks to pass through. Observationally, the cellular concrete with 60% porosity dissipates dynamic load through the fracture and collapse of the pore wall.

3.2. Stress–Strain Relationship

3.2.1. Quasistatic Stress–Strain Relationship. As shown in Figure 16 and Table 4, the cellular concrete specimens with lower porosity exhibited a greater strength and elastic

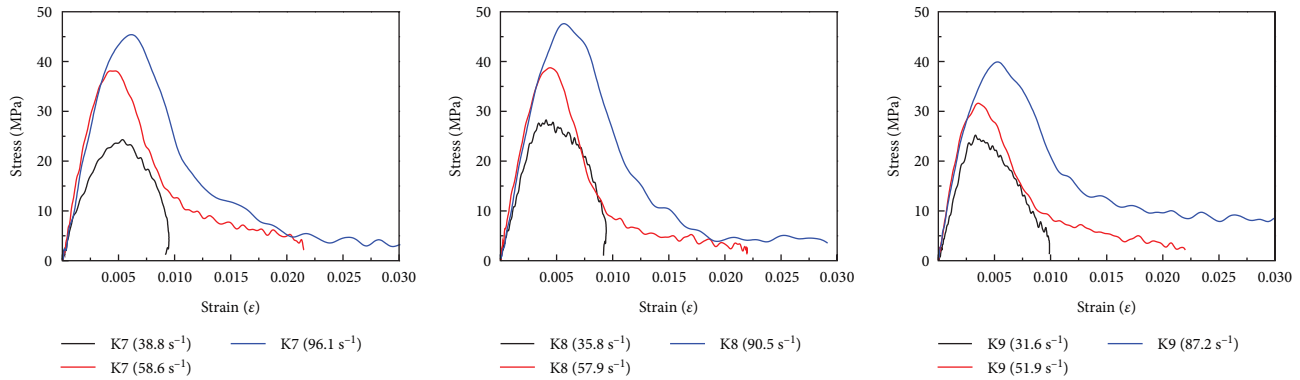

Figure 9: Dynamic stress–strain curves for cellular concrete with 60% porosity and PPF.

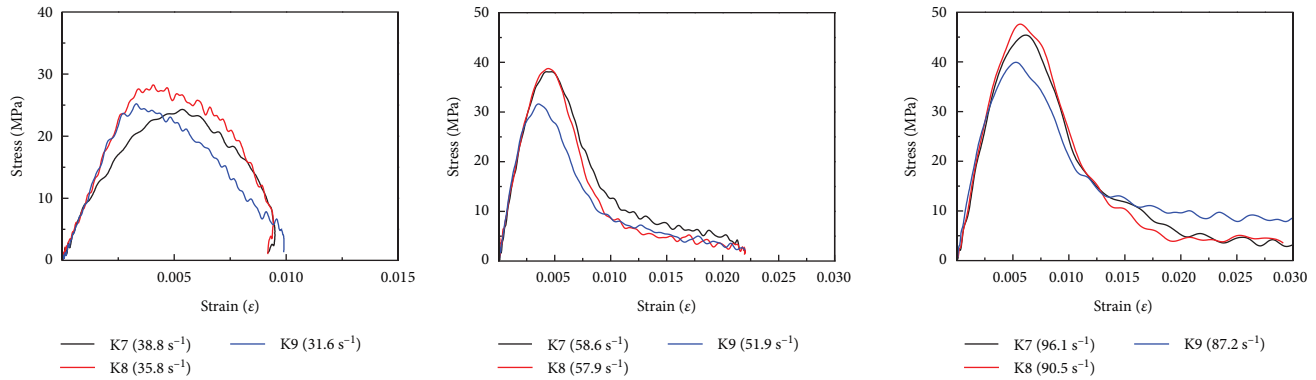

Figure 10: Effect of PPF content in cellular concrete with 60% porosity under the same loading.

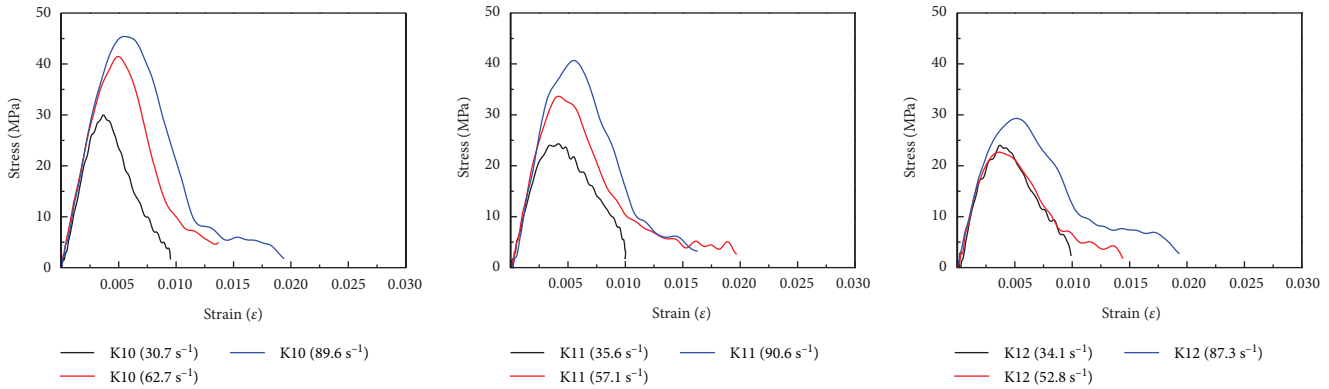

Figure 11: Dynamic stress–strain curves for cellular concrete with 60% porosity and BF.

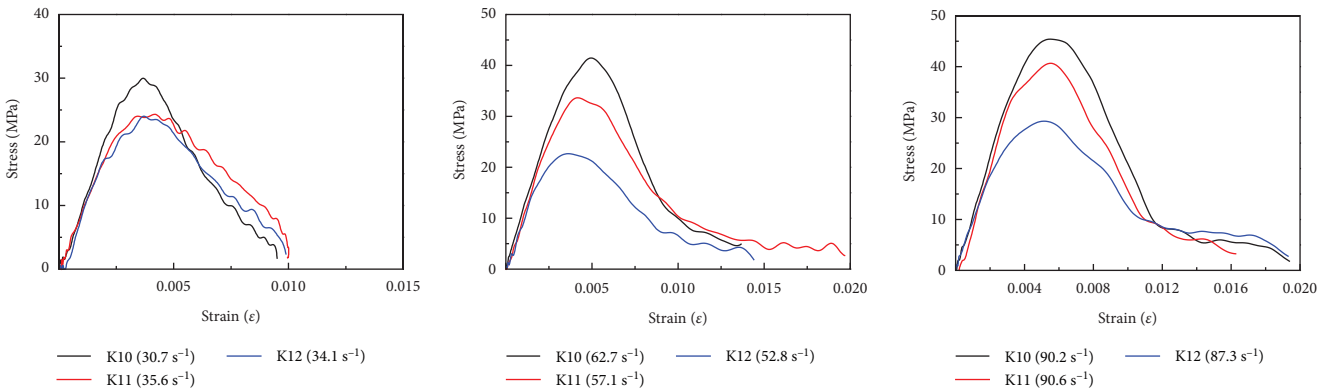

Figure 12: Effect of BF content in cellular concrete with 60% porosity under the same loading.

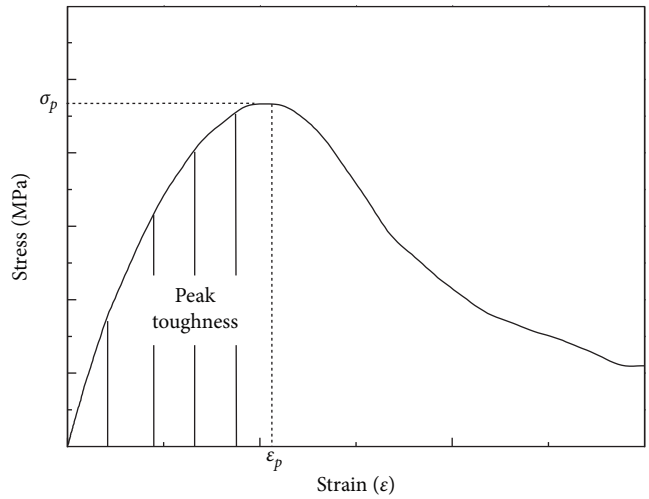

Figure 13: Schematic for peak toughness in stress–strain curve.

Figure 14: Failure of cellular concrete under impact loads.

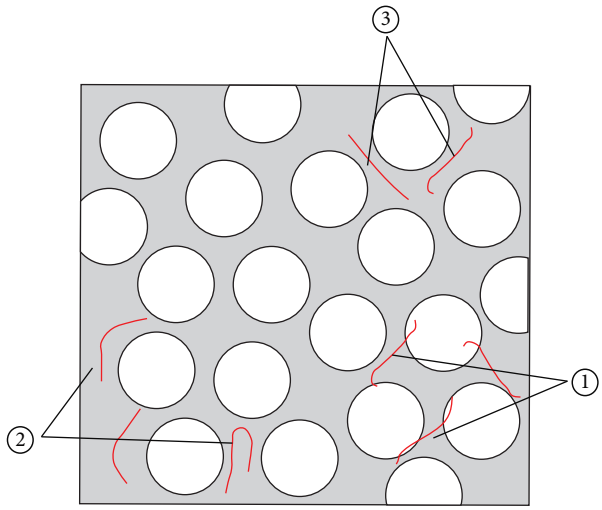

Figure 15: Shapes of fibers in cellular concrete.

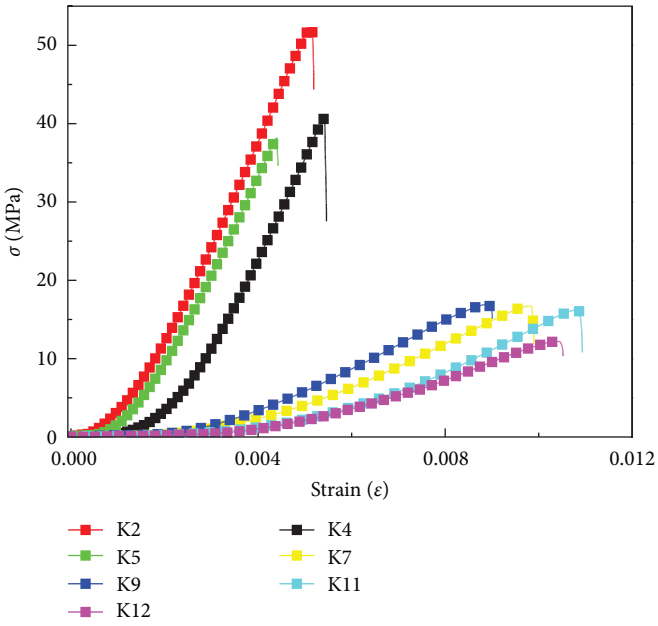

Figure 16: Strain–stress curves of quasistatic compressive test for cellular concrete.

modulus, approximately thrice that with 60% porosity. Compared to normal concrete with similar strength, the cellular elastic modulus of concrete is only 1/2–2/3 of it. The cellular concrete with 60% porosity showed similar internal structural characteristics and elastic modulus to foamed concrete with a density of 800 kg/m^3 [32]; however, it had 2.5 times the compressive strength than that of the foamed concrete. Both cellular concrete specimens showed brittle failure characteristics similar to ordinary concrete without pore collapse and compaction process in low-density foamed concrete under static pressure. Changing the fiber type and content had a great influence on the quasistatic strength of the cellular concrete without prominent impacts on its elastic modulus. The quasistatic compressive strength increases firstly and

Table 4: Quasistatic compressive test results for cellular concrete.

ID	$f_{quasi.c}$ (MPa)	E_{quasi} (MPa)	R_{quasi} (MJ/m^3)
K1	46.8	13,061.89	0.0908
K2	52.2	13,153.05	0.1130
K3	34.9	12,003.69	0.0602
K4	47.3	14,028.55	0.0701
K5	37.6	12,856.41	0.0597
K6	36.0	12,229.59	0.0649
K7	17.0	2,944.39	0.0551
K8	19.0	3,085.16	0.0742
K9	16.9	3,014.11	0.0532
K10	15.3	3,023.57	0.0521
K11	14.9	2,844.74	0.0477
K12	13.5	2,668.11	0.0407

then decreases with the increase of PPF content. The BF made quasistatic compressive strength decreases gradually with more fiber added. While, the variation trend of toughness was consistent with that of quasistatic strength. The difference caused by fiber mainly originated from the balance between crack resistance and the initial defects both introduced by fibers, which was related to its morphology, affinity, and amount of the fiber. The dosage of fiber may be optimum for PPF concrete but might be excessive for BF concrete. It was proved that PPF can improve the performance of concrete to resist early crack, but does little to improve other properties [21–23] for its relatively lower tensile strength and modulus, especially with low dosage. Thus more fiber was needed to maintain the bearing to stress and deformation after cracking. BF might induced more defects than PPF with the same dosage. Finer BF caused more quantities and specific surface areas, which means more interfaces between fibers and matrix. Combined with the hydrophobic property of BF, the thickening effect improved the viscosity of concrete and difficult to discharge air in the process of pouring, which induced more defects.

High-dosage PPF makes a sharp decrease of the elastic modulus, while achieving a relative integral failure appearance. With 1 vol% BF, two kinds of cellular concrete acquired a reduction of 26.4% and 12% in quasistatic compressive strength than concrete with less fiber. Therefore, the cellular concrete under static load should be selected with medium content (0.6 vol%) of PPF and low content (0.2 vol%) of BF to enhance strength.

3.2.2. Dynamic Stress–Strain Relationship. It could be observed in the stress–strain curves that the strain rate and dynamic peak stress increased with the increase of impact load, indicating a significant strain-rate effect of all series of specimens. Among which, the cellular concrete with porosity of 60% achieved higher strain rate due to its lower strength and elastic modulus under the impact of the same velocity.

As shown in Figures 5–8, the curves of the cellular concrete with 20% porosity have a "back stage," that is the positive slope of the downward section of the curve. The value at the intersection of the tangent line at the end and the strain

axis is less than the peak strain, demonstrating inconspicuous strain softening under low-speed impacting. The recovery after unloading was also detected in a dynamic test on steel fiber concrete [20], UHPC [33], and EPS concrete [34]. Under sufficient small loading, cellular concrete can exhibit elastic recovery regardless of porosity. This indicates that the damage accumulation of the cellular concrete is small with nonsignificant plastic development. In general, the strain-rate boundary of the change of the curves' shape can be called the sensitive threshold. Combined with the failure phenomena in Figure 14, specimens with 20% porosity, show the dynamic characteristics from core-reserve failure to fracture failure, meaning the strain rate does not exceed the sensitive threshold of the cellular concrete [20]. It demonstrated that the strain-rate sensitive threshold of the cellular concrete with 20% porosity is between 17 and 50 s^{-1}. The K1–K6 series exhibited similar failure characteristics. The sensitive segment of strain rate is the same, although mixture design has large variation.

While, for both types of fiber, the amount of fiber changed the distance of increasing stage and descending stage, which reflected the maintenance of elastic properties. With the increase in fiber content, it was first strengthened and then weakened. Fibers' effect of bridging and force transferring reduced the generation and development of cracks, formed connection of concrete fragments, and absorbed the impact energy. While the effect of fiber is more obvious in concrete with lower porosity due to more matrix and less likely to cause defects.

Under the same low-speed impact, the curve shape of the cellular concrete with 60% porosity is more "plump" without a "back stage." High porosity reduced the sensitive threshold of strain rate and improved the sensitivity to dynamic load. With a low strain rate (40 s^{-1}), the descending section of the stress–strain curves of the K7–K12 series presented a "bulge," which directly reflected the evident anticracking effect of fibers, indicating that fibers can still bridge and transfer load after cracking of concrete. In descending stage, the brittle random response was also weakened accordingly. The "Back stage" phenomenon might not represent the effect of energy dissipation capacity, but the different mechanisms of various concrete with different porosity. The energy absorption of the cellular concrete with high porosity is not achieved by maintaining its elastic deformation, but by cracking and crushing.

3.3. Strain-Rate Effect. The DIFs of all specimens with various fiber content and impact loads were plotted. One broken line represents one strain-rate level, and one color represents one type of specimen with the same porosity and fiber type.

3.3.1. Compressive Strength. As shown in Figure 17, the compressive strength and DIF-f_c of the cellular concrete increased with the increase in strain rate, indicating pronounced strain-rate sensitivity and dynamic enhancement. With the same fiber type and dosage, the cellular concrete with higher porosity achieved a larger strain rate and DIF-f_c. Comparably, foamed concrete can only bear relatively lower strain-rate deformation.

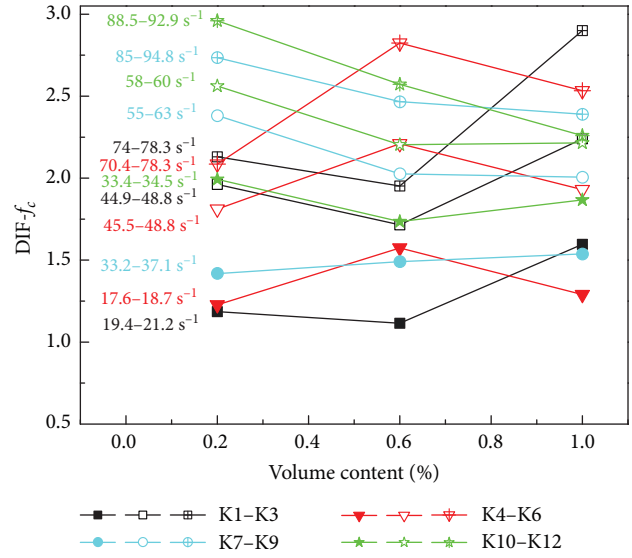

Figure 17: DIF-f_c of cellular concrete.

Fibers offered evident strain-rate enhancement to the cellular concrete. However, with fixed fiber type and porosity, the law of dynamic strength was not evident with the increase in fiber content. In addition, it was difficult to quantify the effect of strain rate on fiber performance and distinguish the contribution of fiber and strain rate to dynamic enhancement. However, the variation in amplitude of DIF-f_c with change in fiber dosage was significant.

The DIF-f_c of cellular concrete with 20% porosity changed more significantly with the fiber content. With more PPF, DIF-f_c of the cellular concrete (K1–K3) decreased slightly and then increased significantly under three levels of impacts. With more BF, the DIF-f_c of the cellular concrete (K4–K6) first increased and then decreased.

However, the change in fiber content did not have a significant effect on the DIF-f_c of the cellular concrete with 60% porosity. Except for the condition of low strain-rate load, the DIF-f_c decreased gradually with the increase in fiber content. For the cellular concrete with lower porosity (K1–K6), PPF could fully devote the reinforcement effect with higher dosage (1 vol%), while BF function best with medium dosage (0.5 vol %). It was revealed that fiber did not enhance the cellular concrete at low dosages, while high dosages might lead to greater weakness. In the cellular concrete with 60% porosity (K7–K12), the enhancement effect of BF was better than that of PPF, especially when low-dosage fiber was added.

The most evident enhancement effect was observed in BF cellular concrete under the highest velocity impact (K4–K6), where the strain-rate effect of BF itself may also provide certain contribution [35]. The strength of some specimens (K10–K12) decreased with an increase of BF, indicating that more original defects were introduced.

Therefore, the porosity and fiber type should be considered when making cellular concrete to make full use of the fiber. The increase in the porosity hindered the expected effects of the fibers. The PPF content of low-porosity cellular concrete should be high (1%), whereas the BF content should

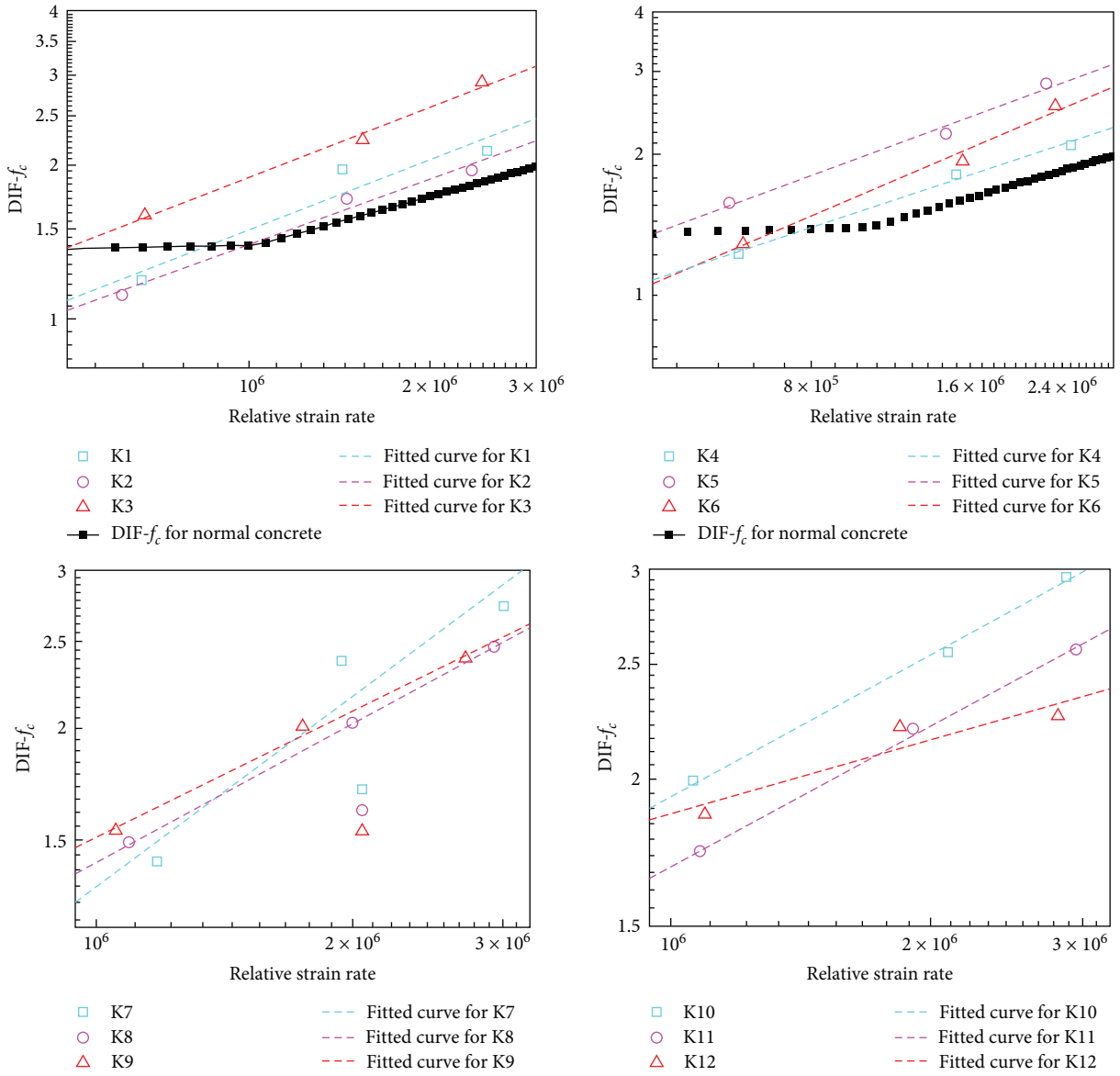

FIGURE 18: Experimental and fitted curves of DIF-f_c with relative strain rate.

be medium (0.6%). The fiber content of the cellular concrete with high porosity should be low (0.2%), whose main function is to build a 3D structure to prevent SAPs from floating.

DIFs are generally expressed as power functions as follows:

$$\mathrm{DIF}-f_c = \frac{f_{\mathrm{Dynamic},c}}{f_{\mathrm{Quasistatic},c}} = \gamma\left(\frac{\dot{\varepsilon}_d}{\dot{\varepsilon}_s}\right)^{\beta}, \tag{5}$$

where $\dot{\varepsilon}_d$ is the strain rate of concrete under dynamic load; $\dot{\varepsilon}_s$ is the strain rate of concrete under quasistatic load, desirable for average strain rate of 3.15×10^{-5}; and β, γ are the parameters to be fitted.

It can be transformed into a linear function form with log $(\dot{\varepsilon}_\mathrm{d}/\dot{\varepsilon}_\mathrm{s})$ as the independent variable and log(DIF-f_c) as the dependent variable in double logarithmic coordinates, which can better describe the relationship between $\dot{\varepsilon}_\mathrm{d}/\dot{\varepsilon}_\mathrm{s}$ and DIF-f_c by linear relationship as follows:

$$\log(\mathrm{DIF}-f_c) = \log\gamma + \beta\log\left(\frac{\dot{\varepsilon}_d}{\dot{\varepsilon}_s}\right). \tag{6}$$

As shown in Figure 18, the DIF-f_c scattered points were fitted in double-logarithmic coordinates using MATLAB. The DIF-f_c of the cellular concrete has a linear relationship with the relative strain rate. The power function accurately described the dynamic enhancement behavior and proved its strain-rate dependency.

The points of DIF-f_c were concentrated and showed strong regularity. Except for the K7 series, the fitted parameters β and γ have the same magnitude. The dynamic response of a high-porosity cellular concrete is relatively discrete, and

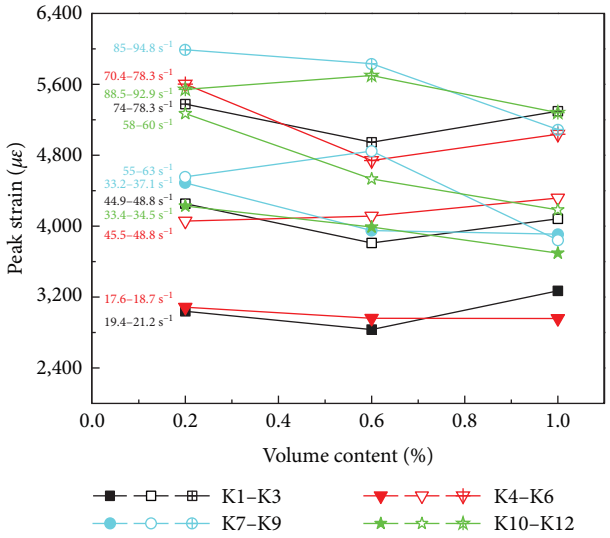

FIGURE 19: Peak strain of cellular concrete under dynamic loads.

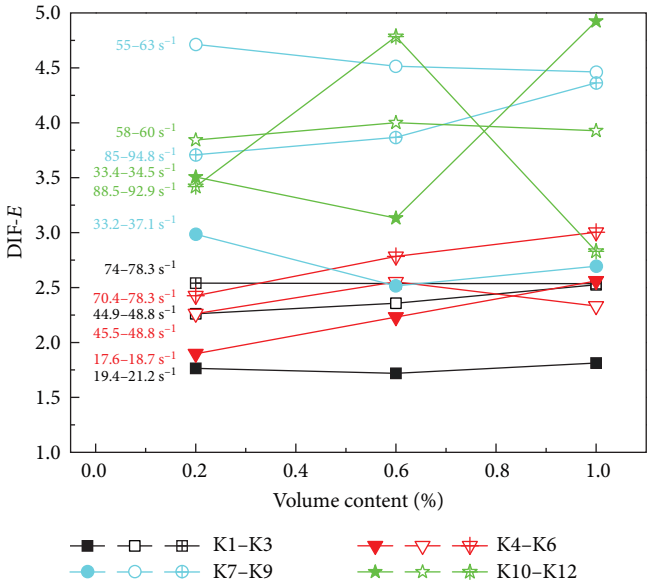

FIGURE 20: DIF-*E* of cellular concrete.

the regularity of fiber is not distinct. According to CEB [36], the DIF-f_c of the C50 normal concrete surges at a relative strain rate over 10^5. However, the cellular concrete exhibited a more evident strain-rate enhancement with an increase in the relative strain rate.

3.3.2. Deformability. The dynamic peak strain and DIF-*E*are shown in Figure 19, which describes the deformability of cellular concrete. In general, the dynamic peak strain and DIF-*E* of all specimens increased with strain rate. The peak strain had a significant strain-rate effect and reached a maximum improvement of approximately 80%.

The peak strain of the cellular concrete was approximately two to three times of ordinary concrete at the same strain-rate level as that of ordinary concrete [37]. The mechanism of the strain-rate effect on the peak strain remains unclear. Owing to errors in specimen processing and experiments, the results of various studies have been inconsistent. Several studies [38, 39] have found that the peak strain of concrete decreases with an increase in the strain rate, or remains basically unchanged. A high strain rate causes the deformation lag behind the strain, leading to enhancement; however, this may reduce the peak strain. For example, the dynamic peak strain of cellular concrete with 60% porosity is smaller than the quasistatic peak strain. However, the addition of fibers can improve the toughness of concrete and may increase the peak strain. The coupling effect is more complicated when the fiber content and porosity are involved. The effect of fiber content on peak strain is not evident, where the peak strain changes by approximately 20% at most with various fiber contents. The fiber certainly improves the deformation ability under low-strain-rate load. High-content PPF significantly increased the peak strain of the cellular concrete with 20% porosity (K1–K6), in which it increased steadily with the increase in fiber dosage. For cellular concrete with more pores (K7–K12), more fiber content decreased the deformability of the concrete. A smaller mortar matrix and a higher proportion of the gas phase in the specimen prevented the toughening and cracking resistance of the fibers. Therefore, to acquire adequate deformability of the cellular concrete with high porosity, a low dosage of fiber should be added. The influence of fiber type on the peak strain of the cellular concrete with 20% porosity was not evident. However, 60% porosity cellular concrete which showed a pronounced effect on the peak strain, as shown in the discrete experimental results.

As shown in Figure 20, the DIF-*E* of cellular concrete with 20% porosity increased with an increase in the fiber content. The enhancement of the BF was slightly stronger than that of the PPF. The dynamic modulus of the K1–K3 series did not increase evidently with the increase in PPF content. Meanwhile, the dynamic modulus of the K4–K6 series increased with BF content, mainly because of the greater elastic modulus of the BF. To improve stiffness, high-content BF should be added to 20% porosity cellular concrete. The smaller static elastic modulus of the 60% porosity cellular concrete results in a higher strain rate and greater DIF-*E*, indicating that the elastic modulus is also more sensitive to high strain rates. However, the influence of fiber is also more prominent and complex and is closely related to the strain rate level. There was a situation of discrete test data, which also indirectly indicated that the role of fiber is not fully utilized.

The DIF-*E* was also fitted in double logarithmic coordinates, as shown in Figure 21. The experimental data for the dynamic elastic modulus of cellular concrete with 20% porosity (K1–K6) were more concentrated. The DIF-E had a linear relationship with the strain rate, indicating that it was a strain-rate stiffening material. In addition, owing to the discrete results of cellular concrete with 60% porosity (K10–K12), the strain-rate effect could not be described as a power function. Although the change in the peak strain was not evident, the elastic modulus generally increased with a strain rate. Microdamage continuously accumulated and

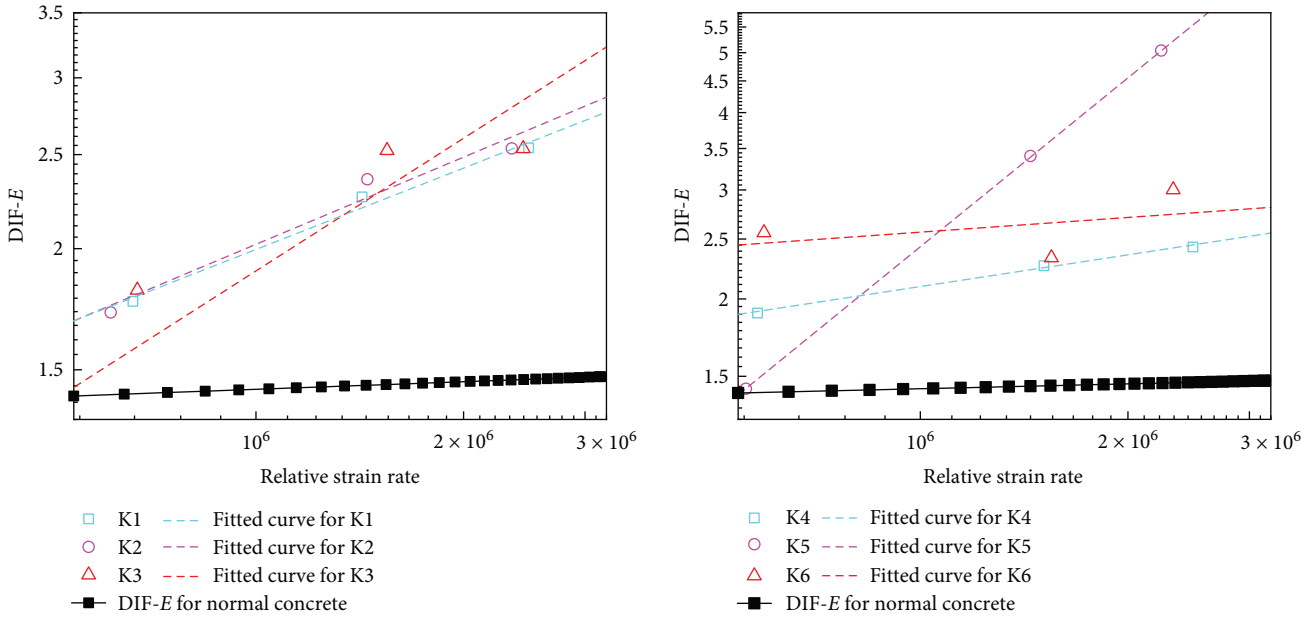

Figure 21: Experimental and fitted curves of DIF-E versus relative strain rate.

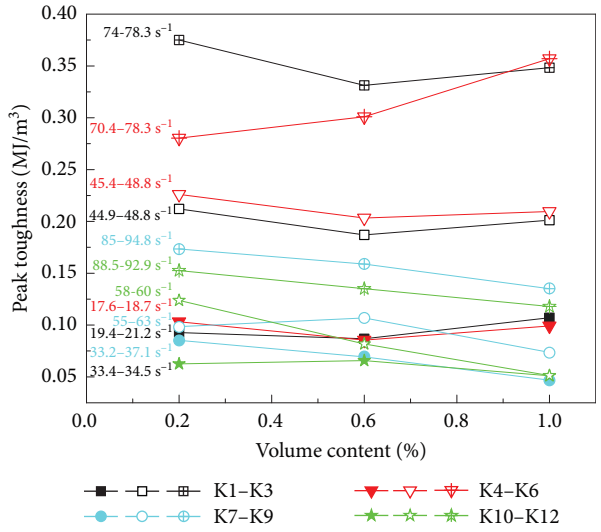

Figure 22: Peak toughness of cellular concrete under dynamic loads.

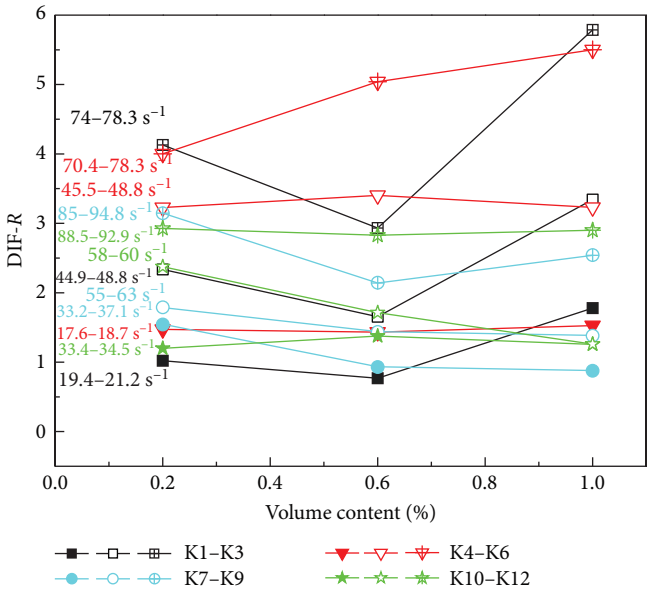

Figure 23: DIF-R of cellular concrete.

evolved during dynamic loading, which led to strain softening. Therefore, the dynamic elastic modulus is not only related to the strain rate, but also to the loading history.

Generally, an expression for the DIF of only secant elastic modulus or initial elastic modulus is proposed [40]. The CEB [36] proposed the formula as $\mathrm{DIF}-E=(\dot{\varepsilon}_d/\dot{\varepsilon}_s)^{0.026}$, where $\dot{\varepsilon}_s=3\times10^{-5}$. As the strain rate increased, the DIF-E of ordinary concrete was always less than 1.5, whereas that of the cellular concrete was larger, indicating a higher sensitivity to the strain rate.

3.3.3. Energy Absorption. Peak toughness and DIF-R are presented in Figures 22 and 23 and show the characterization of the energy absorption capacity. The peak toughness increased with an increase in strain rate in all specimens. This was due to the influence of porosity. Toughness is a comprehensive representation of strength and deformability. The lines of the K7–K12 series were concentrated in the lower part of the coordinate system.

Even with high strain rate and large deformation, the strength of the cellular concrete with porosity of 60% (K7–K12) was very small, resulting in poor energy absorption. Increasing the fiber content did not improve energy absorption. A higher fiber content might have a reverse effect, which is consistent with the characteristics of the compressive strength and peak strain of the cellular concrete

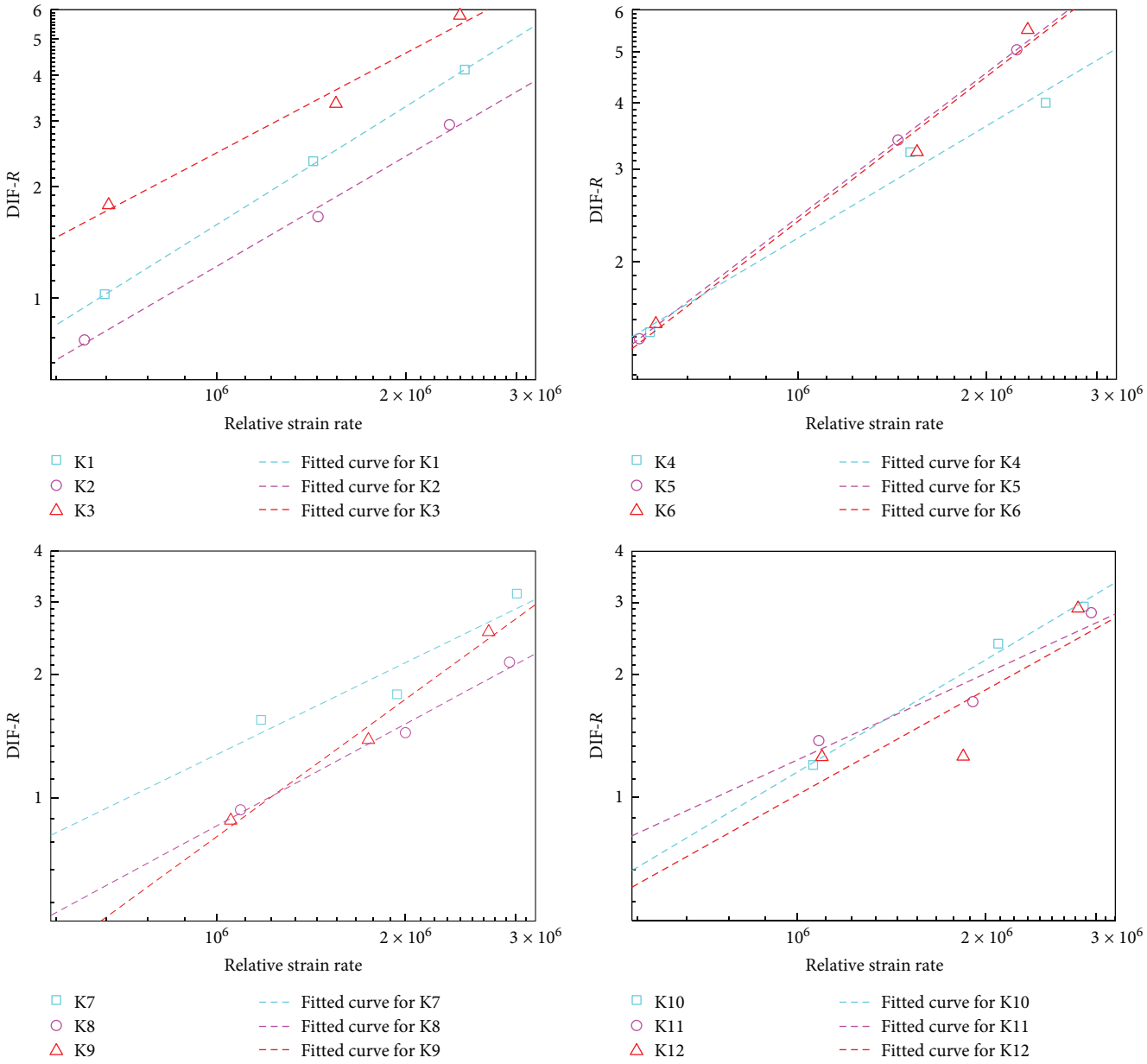

Figure 24: Experimental and fitted curves of DIF-R versus relative strain rate.

with 60% porosity. Owing to the significant increase in strength, the peak toughness of the cellular concrete with porosity of 20% was significantly greater than that with a higher porosity under similar loads. The effect of fiber on the peak toughness is more evident for the cellular concrete with 20% porosity, especially under higher strain-rate loads. High-dosage BF offered more in of toughness, while PPF worked better at low dosages.

The DIF-R reflected the strain-rate effect of the energy absorption capacity. It increased significantly with the effect of fiber and high strain-rate loads, approximately six times that under quasistatic loads. Similar to the dynamic elastic modulus, although a higher porosity cause the cellular concrete achieve a larger strain rate, the peak toughness was not sensitive to the strain rate compared to the lower-porosity specimens. The effect of fiber was also indistinctive, with the reverse effect detected at higher fiber content. For the cellular concrete with 20% porosity, the fiber type was the key factor, especially under higher strain-rate load. The peak toughness of the cellular concrete with BF was more sensitive to the strain rate than that with PPF. With an increased PPF dosage, the DIF-R first decreased and then increased. However, it increased steadily with an increase in BF. The enhancement of the two types of fiber was similar as that with the highest fiber content. It also highlighted the rigidity of fiber, which cannot be ignored because of the different results of various fibers. Hence, for cellular concrete with 20% porosity, the fiber should be maintained at a high content (2%) to enhance the toughness.

As shown in Figure 24, the DIF-R was also fitted as Equation (6) and could be well described by a power function. There is a linear relationship between DIF-R and the

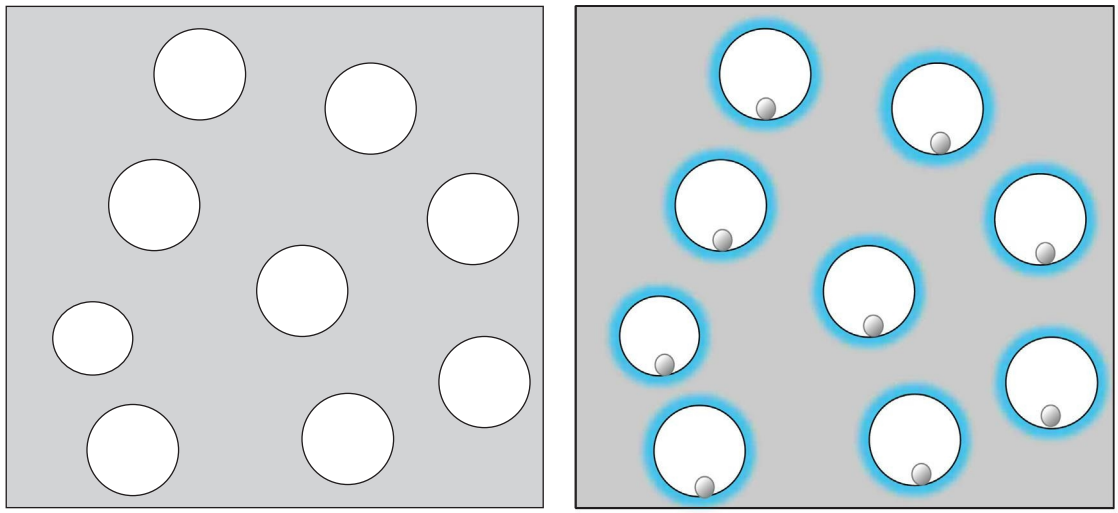

Figure 25: Ordinary pores and internal cured pores [42].

relative strain rate in double logarithmic coordinates, indicating that cellular concrete is a rate-dependent toughening material.

4. Dynamic Mechanical Behavior Mechanism

4.1. Failure Mechanism. The failure of concrete under dynamic load was manifested as cracks, and the initial microcracks or lacuna gradually extended, regenerated, and connect. During transient loading, each infinitesimal body inside cannot deform as a quasistatic equilibrium of the force and displacement. The transition from the stress state to the strain state causes a time difference, that is, the inertia effect [41]. Macroscopically, the deformation of the specimen lagged behind load transmission. It is the only method that consumes energy by increasing the stress and generating more new cracks to cope with dynamic loads, according to the functional principle. Fracture mechanics also showed that the energy required for crack formation is much higher than that required for crack development. Thus, more cracks resulted in more energy being absorbed. This explains the significant improvement in the strength and elastic modulus of the cellular concrete under dynamic loads. Cracks generally develop along the weak interface between mortar and gravel, namely, the interfacial transition zone (ITZ). Under dynamic loads, cracks may directly pass through gravel, resulting in higher energy consumption.

4.2. Effect of Pores. The internal structure of cellular concrete is also conducive to its strain-rate enhancement. As shown in Figure 25, the moisture in the SAPs continuously exerts and causes secondary hydration on the cementitious material around the spherical pores, forming a dense enhanced layer with a thickness of 2–3 mm [42] and can be regarded as the "inner curing zone." Its microhardness was tested to be approximately twice of the outside of the "inner curing zone." In addition, there is no typical ITZ in the cellular concrete. Therefore, under static loading, cracks develop along the mortar matrix between the spherical pores without an evident stress concentration. Under dynamic loading, the stress waves interact at different positions in a two-phase mixture of gases and solids. The complex transmission and reflection between the hollow spherical pores formed an uneven stress field inside.

The fracture path changes continuously and in a complex manner during the propagation of the stress wave. This also required more time to get from the unstable state to the equilibrium state. In addition, the effect of the compression and tensile waves generated on the inner wall of pores also cause it to rupture and collapse, where cracks would directly pass through. With increasing dynamic load, the change in crack path and failure of spherical pores, accompanied by the accumulation of microcracks, increased the energy consumption strength with strain rate, which also explains the crumble failure.

4.3. Effect of Fibers. Fibers provide reinforcement, crack resistance, and toughness to concrete, which are closely related to their physical and chemical properties, mechanical properties, morphological characteristics, and dispersion in concrete. Fibers build 3D structures to realize the uniform distribution and rheological stability of SAPs. The randomly distributed fiber also divided the concrete into small units and constructed a frame to transfer the load and optimize the anisotropic mechanical performance. Therefore, the failure fragments were flocculent structures connected by fibers, particularly in cellular concrete with a porosity of 20%. As shown in Figure 15, the cellular concrete obtained better integrity and homogeneity than ordinary concrete, while it provided less matrix and space for fiber to freely distribute and deform with high porosity. Inside fibers are difficult to distribute and created lapping. As analyzed in Section 3.1, the undesirable distribution is inadequate to withstand the cracking stress. Excessive fibers easily introduce original

defects, especially to mortar pore wall, and result in stress concentration, hindering the development of dynamic strength.

PPF has a fine diameter (average 51 μm) and great dispersion in cementitious materials, which provides cracking resistance and non-negligible thickening, interface effect, and load transfer [43]. Crack resistance refers to the suppression of microcracks, such as dry shrinkage and creep, to achieve better integrity and strength, which could also improve dynamic performance [22]. This is related to the spacing and fineness of the fibrils, as finer diameter and smaller spacing can work better. The load-transfer effect is also a reinforcement of concrete and manifests as a constraint on the cracks. This is helpful in improving the toughness of the strength and ductility of the material.

However, PPF can only prevent cracking from dry shrinkage and condensation or under low strain-rate deformation, especially when a low-dosage fiber is added, because of its relatively smaller elastic modulus and tensile strength. Thus, less fiber had little effect on the improvement of toughness and retention of the strength and stiffness after cracking. Experiments confirmed that after cracking, the toughness and energy absorption were improved with more than 0.2 wt% fibers [44], particularly in the fabrication of high-strength concrete.

BF has greater tensile strength and modulus than PPF, which offered a better load-transfer effect and enhancement in both strength and stiffness. Moreover, after the failure of cellular concrete, BF can still transfer load with its pull-out process to absorb energy. However, the dispersion and posture of the fiber have important influence on the pull-out process and, consequently, on the dynamic enhancement of cellular concrete.

With more BFs, the thickening effect increased the viscosity of the mixture and the difficulty of pouring compaction. When it comes to low water–cement ratio mixtures, more defects are introduced that are detrimental to the generation of strength. The higher fineness of BF increased the number of fibrils and specific surface area, leading to a larger fiber-matrix interface area. Along with its hydrophobic property, the water–cement ratio at the interface is larger where more defects develop. The above analysis explained the decrease of strength and energy absorption of the cellular concrete with higher porosity or more BFs.

The strain rate of the fibers may influence the dynamic performance of concrete. It was found that in PPF concrete, fiber did not work under a strain rate of over 100 s^{-1}. The strain rate threshold can be improved by increasing the dosage, diameter, or elastic modulus of the fiber. Therefore, the synergistic effect of PPFs can be utilized with high dosages [22]. BFs have been proven to have a significant strain-rate effect with an increase in strength and elastic modulus under dynamic loads. It is preferable to optimize the dynamic mechanical properties of cellular concrete and explain the more prominent changes in DIF-f_c and DIF-R with varying fiber content.

5. Conclusions

A novel cellular concrete fabricated with SAPs was introduced for possible applications as an energy-absorbing material. Using an SHPB device, 12 series of cellular concretes with various porosities, fiber types, and fiber amounts were tested under dynamic loads. Based on the results and discussion, the following conclusions were drawn:

(1) Cellular concrete performs similarly to normal concrete under a quasistatic compressive load with brittle failure but a lower elastic modulus. Its strength, modulus, and peak toughness are clearly improved with the increase of strain rate. The relationships between the dynamic DIF and strain rate can be well fitted through power function equations.

(2) The strain-rate enhancement of cellular concrete originated from the following four aspects: development of initial crack lag behind the generation of new cracks, inertia effect of cellular concrete, complicated changes in the stress field and crack path caused by special structures, and deformation and cracking of locally enhanced pores.

(3) Fibers evidently influence the mechanical properties, including strength, stiffness, and toughness. Their regularities were more evident in the cellular concrete with porosity of 20%. The amount of fibers, physicochemical properties, distribution, and shape can lead to weakening or enhancing effects on cellular concrete through their thickening effect, interface reaction, and force transmission.

(4) Recommended fiber types and dosages were proposed for different purposes. To improve strength, low-porosity cellular concrete requires high-content (1%) PPF or medium-content (0.6%) BF. High-porosity cellular concrete requires low-content fiber (0.2%). To improve stiffness, low-porosity cellular concrete requires a high-content (1%) BF.

The cellular concrete investigated above is a heterogeneous composite material with a complex stress field under dynamic loading. In further research, more methods should be adopted to analyze its mechanical laws, influencing factors, and microscopic mechanisms. Meanwhile, more parameters affecting dynamic mechanical properties could be included such as pore size, hybrid fiber, and matrix properties.

Data Availability

The data used to support the findings of this study are available from the corresponding author upon request.

Conflicts of Interest

The authors declare no conflict of interest. The funders had no role in the design of the study; in the collection, analyses,

or interpretation of data; in the writing of the manuscript; or in the decision to publish the results.

Acknowledgments

This research was funded by the Natural Science Foundation Project of Chongqing, grant number cstb2022BSXM-JSX0023 and cstc2021jcyj-msxmX0131; the Science and Technology Research Program of Chongqing Municipal Education Commission, grant number KJZD-K202212902.

References

[1] J. R. Ren, Z. P. Deng, L. Zhou, and X. H. Zheng, "Numerical simulation of dynamic mechanical properties of porous concrete fabricated with the SAP," *Modelling, Measurement and Control B*, vol. 86, no. 2, pp. 535–556, 2017.

[2] T. T. Nguyen, H. H. Bui, T. D. Ngo, and G. D. Nguyen, "Experimental and numerical investigation of influence of air-voids on the compressive behaviour of foamed concrete," *Materials & Design*, vol. 130, pp. 103–119, 2017.

[3] G. C. Hoff, *Shock-Absorbing Materials. Report 1. Backpacking Materials for Deeply Buried Protective Structures*, Waterways Experiment Station, Vicksburg, MS, 1967.

[4] E. L. Bai, J. Y. Xu, and Z. G. Gao, "Study on deformation property of EPS concrete under impact loading," in *Proceedings of the International Conference on Green Building, Materials and Civil Engineering (GBMCE 2011)*, Shangri La, People's Republic of China, August 22–23, 2011.

[5] S. Lu, J. Y. Xu, X. Luo, Z. G. Dong, and H. W. Wang, "Dynamic features experiment of hollow corundum ball concrete," *Journal of Vibration and Shock*, vol. 35, no. 12, pp. 110–116, (in Chinese), 2016.

[6] J. Shen and X. J. Ren, "Experimental investigation on transmission of stress waves in sandwich samples made of foam concrete," *Defence Technology*, vol. 9, no. 2, pp. 110–114, 2013.

[7] Q. Q. Guo, Y. B. Gou, J. Chen, Y. Zhang, and Y. Zhou, "Dynamic response of foam concrete under low-velocity impact: experiments and numerical simulation," *International Journal of Impact Engineering*, vol. 146, Article ID 103693, 2020.

[8] S. Feng, Y. Zhou, Y. Wang, and M. Lei, "Experimental research on the dynamic mechanical properties and damage characteristics of lightweight foamed concrete under impact loading," *International Journal of Impact Engineering*, vol. 140, Article ID 103558, 2020.

[9] L. L. Wang, L. M. Yang, and F. H. Zhou, "On flexible protection and stiff protection for structure safety under explosive/impact loading," *Explosion and Shock Waves*, vol. 29, no. 4, pp. 337–344, (in Chinese), 2009.

[10] W. M. Li and J. Y. Xu, "Mechanical properties of basalt fiber reinforced geopolymeric concrete under impact loading," *Materials Science and Engineering: A*, vol. 505, no. 1-2, pp. 178–186, 2009.

[11] F. S. Rostásy and K. Hartwich, "Compressive strength and deformation of steel fibre reinforced concrete under high rate of strain," *International Journal of Cement Composites and Lightweight Concrete*, vol. 7, no. 1, pp. 21–28, 1985.

[12] G. Chen, D.-P. Zheng, Y.-W. Chen et al., "Development of high performance geopolymer concrete with waste rubber and recycle steel fiber: a study on compressive behavior, carbon emissions and economical performance," *Construction and Building Materials*, vol. 393, Article ID 131988, 2023.

[13] J.-X. Lin, J.-Y. Su, H.-S. Pan et al., "Dynamic compression behavior of ultra-high performance concrete with hybrid polyoxymethylene fiber and steel fiber," *Journal of Materials Research and Technology*, vol. 20, pp. 4473–4486, 2022.

[14] C. Gong, L. Kang, M. Cheng, and M. Lei, "Parameter modification and extension of the compressible packing model (CPM) for steel fiber-aggregate mixtures," *Powder Technology*, vol. 422, Article ID 118479, 2023.

[15] C. Gong, L. Kang, L. Liu, M. Lei, W. Ding, and Z. Yang, "A novel prediction model of packing density for single and hybrid steel fiber-aggregate mixtures," *Powder Technology*, vol. 418, Article ID 118295, 2023.

[16] E. Monaldo, F. Nerilli, and G. Vairo, "Basalt-based fiber-reinforced materials and structural applications in civil engineering," *Composite Structures*, vol. 214, pp. 246–263, 2019.

[17] J.-X. Lin, Y. Song, Z.-H. Xie et al., "Static and dynamic mechanical behavior of engineered cementitious composites with PP and PVA fibers," *Journal of Building Engineering*, vol. 29, Article ID 101097, 2020.

[18] Y.-Q. Peng, D.-P. Zheng, H.-S. Pan et al., "Strain hardening geopolymer composites with hybrid POM and UHMWPE fibers: analysis of static mechanical properties, economic benefits, and environmental impact," *Journal of Building Engineering*, vol. 76, Article ID 107315, 2023.

[19] M. A. Rasheed and S. S. Prakash, "Behavior of hybrid-synthetic fiber reinforced cellular lightweight concrete under uniaxial tension—experimental and analytical studies," *Construction and Building Materials*, vol. 162, pp. 857–870, 2018.

[20] N. I. Karpenko, A. V. Mishina, and V. I. Travush, "Impact of growth on physical, mechanical and rheological properties of high strength steel fiber reinforced concrete," in *24th Russian-Polish-Slovak Seminar on Theoretical Foundation of Civil Engineering*, pp. 390–397, Elsevier Science BV, 2015.

[21] B. Du, H. W. Ma, and L. Lin, "Dynamic split tension and energy dissipation of fiber concrete under impact loading effect," in *International Conference on Electromechanical Control Technology and Transportation (ICECTT)*, pp. 91–100, Atlantis Press, 2015.

[22] R. Sridhar and R. Prasad, "Mechanical and dynamic properties of polypropylene fiber reinforced concrete," in *2nd Quadrennial International Conference on Structural Integrity (ICONS)*, pp. 361–374, Springer Singapore, 2018.

[23] K. Zieliński and P. Olszewski, "The impact of basaltic fibre on selected physical and mechanical properties of cement mortar," *Betonwerk und Fertigteil-Technik/Concrete Precasting Plant and Technology*, vol. 71, no. 3, pp. 28–33, 2005.

[24] W. Li and J. Xu, "Impact characterization of basalt fiber reinforced geopolymeric concrete using a 100-mm-diameter split Hopkinson pressure bar," *Materials Science and Engineering: A*, vol. 513-514, pp. 145–153, 2009.

[25] F. L. Fan, J. Y. Xu, E. L. Bai, and Q. He, "Experimental study on impact-mechanics properties of basalt fibre reinforced concrete," *Advanced Materials Research*, vol. 168-170, pp. 1910–1914, 2010.

[26] L. Ying and L. Kai-Xin, "Characteristic analysis for stress wave propagation in transversely isotropic fluid-saturated porous media," *Applied Mathematics and Mechanics*, vol. 25, no. 6, pp. 656–663, 2004.

[27] Z. Deng, H. Cheng, Z. Wang, G. Zhu, and H. Zhong, "Compressive behavior of the cellular concrete utilizing

millimeter-size spherical saturated SAP under high strain-rate loading," *Construction and Building Materials*, vol. 119, pp. 96–106, 2016.

[28] F. Wang, J. Yang, H. Cheng, J. Wu, and X. Liang, "Study on mechanism of desorption behavior of saturated superabsorbent polymers in concrete," *Aci Materials Journal*, vol. 112, no. 3, pp. 463–470, 2015.

[29] N. A. Soliman and A. Tagnit-Hamou, "Partial substitution of silica fume with fine glass powder in UHPC: filling the micro gap," *Construction and Building Materials*, vol. 139, pp. 374–383, 2017.

[30] G. Sanjayan and L. J. Stocks, "Spalling of high-strength silica fume concrete in fire," *ACI Materials Journal*, vol. 90, no. 2, pp. 170–173, 1993.

[31] L. Wang, S. Hu, L. Yang et al., "Development of experimental methods for impact testing by combing Hopkinson pressure bar with other techniques," *Acta Mechanica Solida Sinica*, vol. 27, no. 4, pp. 331–344, 2014.

[32] Y. H. M. Amran, N. Farzadnia, and A. A. A. Ali, "Properties and applications of foamed concrete; a review," *Construction and Building Materials*, vol. 101, pp. 990–1005, 2015.

[33] D.-Y. Yoo and N. Banthia, "Mechanical and structural behaviors of ultra-high-performance fiber-reinforced concrete subjected to impact and blast," *Construction and Building Materials*, vol. 149, pp. 416–431, 2017.

[34] Z. B. Hu, J. Y. Xu, G. F. Gao, and S. Cao, "Energy-absorption property of expanded polystyrene concrete under impact," *Journal of the Chinese Ceramic Society*, vol. 38, no. 7, pp. 1173–1178, (in Chinese), 2010.

[35] Y. Yao, D. Zhu, H. Zhang, G. Li, and B. Mobasher, "Tensile behaviors of basalt, carbon, glass, and aramid fabrics under various strain rates," *Journal of Materials in Civil Engineering*, vol. 28, no. 9, pp. 1–10, 2016.

[36] C. E.-I. D. Beton, "CEB-FIP model code 1990," 1993.

[37] P. Liu, X. Han, D. Hu, and C. Jiang, "Sensitivity and uncertainty analysis of SHPB tests for concrete materials," *International Journal of Applied Mechanics*, vol. 163, pp. 414–427, 2018.

[38] A. Bagher Shemirani, R. Naghdabadi, and M. J. Ashrafi, "Experimental and numerical study on choosing proper pulse shapers for testing concrete specimens by split Hopkinson pressure bar apparatus," *Construction and Building Materials*, vol. 125, pp. 326–336, 2016.

[39] R. Naghdabadi, M. J. Ashrafi, and J. Arghavani, "Experimental and numerical investigation of pulse-shaped split Hopkinson pressure bar test," *Materials Science and Engineering: A*, vol. 539, pp. 285–293, 2012.

[40] H. Y. Zhou, Y. B. Chen, Y. R. Zhang, and H. Q. Wang, "Research progress of strain-rate effect on mechanical properties of concrete," in *3rd International Conference on Civil, Architectural and Hydraulic Engineering (ICCAHE)*, pp. 1391–1396, Trans Tech Publications, Ltd., 2014.

[41] X. Chen, S. Wu, J. Zhou, Y. Chen, and A. Qin, "Effect of testing method and strain rate on stress–strain behavior of concrete," *Journal of Materials in Civil Engineering*, vol. 25, no. 11, pp. 1752–1761, 2013.

[42] J. Yang, F. Z. Wang, and Y. P. Liu, "Comparison of ordinary pores with internal cured pores produced by superabsorbent polymers," *Advanced Materials Research*, vol. 1129, pp. 315–322, 2015.

[43] W. H. Xuan, Y. Wang, and Y. Z. Chen, "Microcosmic analysis on bonding performance of polypropylene fiber concrete," *Advanced Materials Research*, vol. 168-170, pp. 2150–2153, 2010.

[44] S. J. Wang, X. Zhu, W. Wang, and J. Li, "The analysis on how the polypropylene fiber reinforced concrete works," *Advanced Materials Research*, vol. 163-167, pp. 4580–4584, 2010.